Within-field crop leaf area index simulation using a hybrid PROSAIL-SVR approach: evaluating Sentinel-2 and PlanetScope potential

Rahul Raj, Bagher Bayat, Ahsan Raza, Thomas Gaiser, Harry Vereecken & Carsten Montzka

Published online: 28 Oct 2025.

Submit your article to this journal ⬈

Article views: 593

View related articles ⬈

View Crossmark data ⬈

Taylor & Francis
Taylor & Francis Group

8 OPEN ACCESS · Check for updates

Within-field crop leaf area index simulation using a hybrid PROSAIL-SVR approach: evaluating Sentinel-2 and PlanetScope potential

Rahul Raj [iD][a], Bagher Bayat [iD][a], Ahsan Raza [iD][b], Thomas Gaiser [iD][c], Harry Vereecken [iD][a] and Carsten Montzka [iD][a]

[a]Institute of Bio- and Geosciences: Agrosphere (IBG-3), Forschungszentrum Jülich, Wilhelm-Johnen-Straße, Jülich, Germany; [b]Leibniz Centre for Agricultural Landscape Research (ZALF), Müncheberg, Germany; [c]Institute of Crop Science and Resource Conservation (INRES), University of Bonn, Bonn, Germany

ABSTRACT

Accurate estimation of crop leaf area index (LAI) dynamics at the field scale is crucial in precision agriculture. Crop LAI can directly affect agroecosystem functioning and water use efficiency through evapotranspiration and photosynthesis. An optical radiative transfer model PROSAIL, integrated with satellite remote sensing data, can simulate crop LAI dynamics. Mid-resolution Sentinel-2 and the emergence of novel high-resolution PlanetScope satellite data provide an opportunity to simulate LAI at 10 m and 3 m resolutions, respectively. In this study, we conducted a comprehensive analysis of LAI simulation from both satellite data to explore their potential in capturing within-field LAI variability. We employed a hybrid inversion approach, integrating the PROSAIL model with support vector regression (a machine learning approach), to simulate LAI across different phenological phases of the winter triticale crop in the years 2020 and 2021 at the agriculture field in Brandenburg, Germany, with high spatial variability in crop growth. For validation, ground observations of LAI across the field were obtained, covering different soil classes with varying yield potentials. This allowed us to examine the impact of soil class on LAI development, and we additionally performed a heterogeneity analysis using Rao's Q index to capture within-field variability in simulated LAI. The results showed good accuracy of the simulated LAI from both satellite data, as indicated by Kling-Gupta-Efficiency (KGE) greater than 0.3 threshold and RMSE ranging from 0.48 to 1.51. Although both satellite data showed similar performance in terms of LAI magnitude, PlanetScope showed higher within-field variability and was more sensitive to the yield potential of different soil classes. Rao's Q heterogeneity index map further indicated that PlanetScope captured more detailed and localized variations in LAI compared to Sentinel-2. These findings

CONTACT Rahul Raj ✉ rahulosho@gmail.com; r.raj@fz-juelich.de 🏢 Institute of Bio- and Geosciences: Agrosphere (IBG-3), Forschungszentrum Jülich, Wilhelm-Johnen-Straße, 52425 Jülich, Germany

underscored the respective strengths of mid- and high-resolution satellite data in supporting precision agriculture and highlighted the value of PlanetScope for detailed field-scale applications.

1. Introduction

The goal of precision agriculture is to establish the efficient management of available resources, which increases production and makes agriculture practices more efficient in reducing carbon emissions (DeLay, Thompson, and Mintert 2022; Lowenberg-DeBoer and Erickson 2019; Lower et al. 2022). Monitoring crop status in the agriculture field over the growing period contributes to the aims of precision agriculture. The changes in the crop's biophysical properties are observed during the growth. These changes are often measured as a leaf area index (LAI), defined as the one-sided leaf surface per unit ground surface area (Fang et al. 2019). Precision agriculture leverages LAI observations to optimize field-level management by tailoring agricultural practices such as irrigation, fertilization and spraying to the specific needs of crops in different parts of a field. The crop LAI is highly variable in space and influenced by environmental variables such as soil texture and nutrient availability. LAI is directly linked to water use efficiency, where a higher LAI suggests better utilization of water by crops, leading to understanding crop responses under different irrigation schemes (Paul et al. 2021; Sachin et al. 2023; Shi et al. 2021). Given that photosynthesis drives crop production, the LAI can help manage fertilization and integrate precision agriculture technologies for efficient nutrient distribution (Wang et al. 2023). For spraying, LAI aids in determining the optimal amount of pesticides and herbicides needed, adjusting spray equipment settings for better coverage, and minimizing environmental impact by reducing chemical over-application (Liao et al. 2020; Román et al. 2022). Furthermore, an accurate estimation of LAI is crucial to the process-based model and data synthesis framework that estimates the efficiency of farming practices leading to carbon sequestration by crop (Nevalainen et al. 2022). The total carbon sequestered after harvesting as soil carbon can be converted into carbon credits, generating financial benefits for the farmers. Additionally, LAI can help understand how plants are affected by climate extreme events. High temperatures and prolonged heat waves can lead to increased evapotranspiration rates from crops. Consequently, crops might decrease their leaf area as a water conservation strategy to prevent excessive water loss through evapotranspiration. It could lead to a reduction in the LAI (Laskari et al. 2022). The occurrence of a heatwave can further impact the timing of crop growth and developmental stages, such as leaf emergence and senescence. Occasionally, crops might shed leaves earlier than their normal cycle, influencing the LAI (Burroughs et al. 2022). By monitoring LAI during a heatwave, we can better assess the impact on vegetation and ecosystems and take appropriate action to mitigate any adverse effects.

Field sampling is widely used to observe crop LAI, which is expensive and time-consuming, restricting large-scale and continuous observations. The distributions of LAI are heterogeneous and can be challenging to obtain through field observations alone. Installation of IoT (Internet of Things) devices in the crop field for continuous LAI

observations can also provide reliable data on crop growth (Bauer and Aschenbruck 2018; Yang et al. 2022), but it is still unable to capture the within-field variability. Satellite remote sensing (RS) can observe top-of-canopy (TOC) reflectance by crop and underlying soil background reflectance, providing information on biophysical variables. Radiative transfer models, such as PROSAIL, utilize the biophysical variables to simulate TOC reflectance. Therefore, the inversion of radiative transfer models employing RS observations can provide information on biophysical variables (Gara et al. 2019; Jacquemoud et al. 2009; Verhoef 1998). Such inversion facilitates the simulation of LAI at a field as well as a large spatial scale and provides a cost-effective method to realize crop growth dynamics. While several studies have been conducted using PROSAIL model inversion for crop property estimation at the ecosystem and field scales (Johansen et al. 2022; Kimm et al. 2020; Liu et al. 2024; Pasqualotto et al. 2019; Rosso et al. 2022; Zérah, Valero, and Inglada 2024), further investigation is needed to evaluate how the differing resolutions of satellite data such as Sentinel-2 and PlanetScope can capture within-field variability through model inversion. The multispectral sensor onboard Sentinel-2 satellites delivers TOC reflectance data every five days in 13 spectral bands at a mid-resolution ranging from 10 to 60 m. These bands can be utilized to simulate crop LAI at 10 m resolution. On the other hand, the PlanetScope satellite constellation, consisting of approximately 130 satellites, offers a unique opportunity to simulate crop LAI at a high-resolution of 3 metres, with nearly daily coverage. However, cloud cover and the specific area of interest can impact the effective temporal resolution. Both Sentinel-2 and PlanetScope data can be considered adequate to capture within-field variability, which is effectively represented by spatial heterogeneity, as well as temporal dynamics of the crop. However, the general assumption is that PlanetScope data is more effective at capturing the spatial heterogeneity in terms of LAI compared to Sentinel-2 data due to its higher spatial resolution, allowing for better identification and characterization of small-scale variations in crop cover. In our study, we evaluated the accuracy of both mid-resolution Sentinel-2 data and high-resolution PlanetScope data in simulating crop LAI and capturing the spatial heterogeneity in LAI. We conducted LAI simulation for the winter triticale crop at the Grossmutz agriculture field in Germany across different crop phenological phases, using a hybrid inversion approach that combines the PROSAIL model with machine learning. We showed that this approach works adequately without the need for ground calibration and, therefore, can be applied to different agriculture fields and crop types.

2. Study area

The study was performed at the Grossmutz agriculture experimental field (52 ° 56′ 11.48″ N, 13 ° 7′ 39.74″ E), which is located in the Löwenberger Land, Brandenburg, Germany (Figure 1). The study area covers a small agriculture field around 6.3 ha with variation in elevation from 51.5 to 57.5 m above mean sea level. The study area is characterized by a temperate humid climate with an average rainfall of 550–600 mm yr $^{-1}$ and average relative humidity above 65%. The climatic condition of the study area is characterized by long cold winter and hot summer conditions. The weather station installed in the field recorded an average daily temperature of −1 to 23°C during the sowing and harvesting of winter triticale crop from Sep 2019–July 2020 and Sep 2020–July 2021 (Habib-ur-Rahman
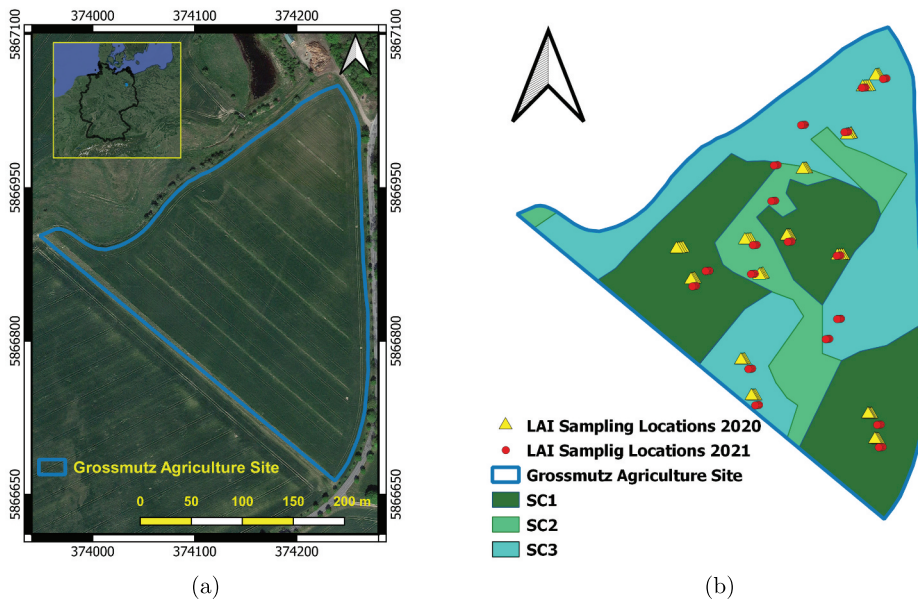
Figure 1. (a) Boundary of the Grossmutz agriculture field in Germany. (b) Soil heterogeneity symbolised by three soil classes: SC1, SC2 and SC3, causing high, medium, and low yield potential, respectively, and sampling locations (14 in 2020 and 18 in 2021) for ground observations of leaf area index (LAI) in three soil classes.

et al. 2022). The total growing season of the crop covers the stages of germination, tillering and stem elongation to ear formation, flowering, and full ripeness. Winter triticale is a hybrid of winter wheat and winter rye, and it is planted for grain production for livestock.

The study area has heterogeneous soil conditions formed from the Glacio-fluvial sediments. The spatial variation in soil texture, which results in varying capacities to hold water, and the variations in topography and elevation, which result in varying soil physical properties, are the sources of soil heterogeneity. Soil mapping was conducted in 2019 using spatially distributed 88 soil samples. At each sampling location, soil profiling was done to the depth of 100 cm to define the horizonation and texture together with the soil organic matter content. These data were used to define the soil map having three classes (SC1, SC2 and SC3) in the study area (Figure 1b). Class SC1 is defined for the soil having an upper boundary of the loamy layer less than 60 cm in the soil profile with a high available water capacity (AWC), leading to high yield potential. Class SC2 belongs to the soil having an upper boundary of the loamy layer in between 60 and 100 cm in the soil profile with moderate AWC leading to moderate yield potential. Class SC3 has no loamy layer in the soil profile (sandy texture throughout) with low AWC leading to low yield potential. Detailed information on soil profiling and soil map generation can be found elsewhere (Habib-ur-Rahman et al. 2022; Raza et al. 2022).

3. Materials and methods

3.1. Ground observations of LAI

The LAI was observed non-destructively with the 'SunScan Canopy Analyser System' (Delta-T Devices Ltd, UK) at 14 sampling locations in 2020 and 18 sampling locations in 2021 to characterize the spatial variation in LAI across the study area (Habib-ur-Rahman et al. 2022). Generally, a SunScan system comprises several sensors affixed to a frame positioned above and below the canopy to detect incident and transmitted radiation. Consequently, intercepted radiation by the canopy provides a direct observation of LAI. The sampling locations were chosen randomly and were distributed over the agriculture field, covering all three soil classes (Figure 1b). Four replicates of LAI were observed at each sampling location, each collected from a 50 cm row segment across four rows within a 1 m^2 plot. The mean of each four replicated LAI was calculated for further analysis. The observations were taken two times each year, belonging to the two winter triticale phenological stages identified by BBCH-code (Biologische Bundesanstalt, Bundessortenamt und CHemische Industrie; Bleiholder et al. (2001)). These selected crop stages for LAI observations were the end of stem elongation phase (BBCH = 39) and the end of flowering (anthesis) phase (BBCH = 69) of the winter triticale. Table 1 summarises the LAI observations (hereafter, LAI$_{obs}$) dates and crop phenological phases.

3.2. Satellite data

We conducted a spatial simulation of LAI within the Grossmutz agriculture field boundary (Figure 1a) on each observation date, utilizing top-of-canopy (TOC) reflectance from both Sentinel-2 and PlanetScope satellite data (Section 3.3). Sentinel-2 satellites are managed by the European Space Agency (ESA) as part of the Copernicus programme. It is a constellation with two identical satellites, Sentinel-2A (launched in June 2015) and Sentinel-2B (launched in March 2017), with a revisit time of five days. Sentinel-2 provides optical image data across a range of spectral bands: four VNIR bands (blue, green, red and near-infrared (NIR) bands) at 10 m, six bands (four red edge bands, two short-wave infrared (SWIR) bands) at 20 m and three bands at 60 m (coastal aerosol, water vapour and cirrus) spatial resolution. PlanetScope comprises a constellation of 130 small satellites (first launched in 2014) orbiting the Earth and is managed by Planet Labs, a private satellite imaging company (Planet Team 2023). These satellites provide daily global coverage with a spatial resolution of 3 m. PlanetScope data are derived from three groups of satellites: Dove Classic and Dove R (four VNIR bands), and Super Dove (eight bands, including additional coastal blue, green 1, yellow, and red-edge bands). We acquired cloud-free and atmospherically corrected PlaneScope and Sentinel-2B data, which were available either on the observation dates or within a six-day interval (either earlier or later) (Table 1). Although there was a six-day gap between the satellite image acquisition and LAI$_{obs}$, this interval was considered acceptable for comparison purposes, as LAI was not expected to vary over such a short period. For instance, the advanced phenological stage of the crop in mid-June 2021 (end of flowering phase) leads to the grain-filling phase, a period during which LAI remains nearly constant and changes only marginally. Moreover, the field observation days were solely determined by the crop growth stages

Table 1. Satellite data and leaf area index (LAI) observations dates. BBCH code is mentioned in Section 3.1. n: number of sampling locations for LAI observations (Figure 1b).

Sentinel-2B acquisition date	PlanetScope acquisition date (Sensor)	LAI observations		Crop phenological phase
		Date	n	
6 May 2020	6 May 2020 (Dove classic)	5 May 2020	14	BBCH=39
15 June 2020	13 June 2020 (Dove classic)	10 June 2020	14	BBCH=69
28 April 2021	28 April 2021 (Dove R)	3 May 2021	18	BBCH=39
10 June 2021	10 June 2021 (Super Dove)	16 June 2021	18	BBCH=69

and favourable sunny conditions. Planet Labs provides PlanetScope TOC reflectance after atmospheric and radiometric corrections as 'analytic_sr' asset, and ESA offers Sentinel-2 TOC reflectance as a Level-2A product. We acquired PlanetScope data from DOVE classic, DOVE-R and SuperDove, and selected the four corresponding VNIR bands. Similarly, we selected the same four VNIR bands at 10 m resolution of Sentinel-2B for LAI simulation.

3.3. LAI simulation from satellite data: hybrid approach

We utilized the optical radiative transfer model PROSAIL (Jacquemoud et al. 2009; Verhoef and Bach 2007), which merges two established models, namely PROSPECT-D (Leaf Optical PROperty SPECTra: Féret and de Boissieu 2024; Féret et al. 2017; Jacquemoud and Baret 1990) and 4SAIL (Scattering by Arbitrarily Inclined Leaves: Verhoef and Bach 2007; Verhoef et al. 2007). PROSPECT-D is capable of simulating the optical properties of individual leaves as a function of the leaf constituents such as chlorophyll content (C_{ab}), dry matter content (C_{dm}), equivalent water thickness (C_w), carotenoids (C_{ca}), and leaf structural components (N). SAIL can simulate the bidirectional reflectance distribution function (BRDF) of vegetation canopies. It considers the geometry of the canopy, such as the average leaf inclination angle (ALIA) and LAI. By merging these two models, PROSAIL simulates the TOC reflectance of vegetation canopies under different conditions, such as varying sun angles, viewing geometries, and canopy architectures. The simulation of LAI can be thought of as an inversion of the PROSAIL model, where the TOC reflectance is available from the satellite data. PROSAIL model has been successfully inverted against hyperspectral laboratory measurements (e.g. Bayat, van der Tol, and Verhoef 2016) and multispectral satellite observations (e.g. Bayat, van der Tol, and Verhoef 2018, 2020; Raj et al. 2020) to simulate the time series of LAI. In the current study, we implemented the PROSAIL model integrated with a support vector regression (SVR: Steinwart and Thomann 2017) method, a machine learning approach, to simulate LAI at each pixel of satellite data. This integration is termed a hybrid inversion approach, which takes advantage of the physical process behind LAI together with machine learning. The hybrid inversion was employed using the R package 'prosail 2.5.2' (Feret and de Boissieu 2024). We implemented the following steps:

(1) We defined the wide uniform distribution of each PROSAIL input parameter based on previously utilized values and observations (Table 2). The upper boundary of LAI distribution was fixed at the maximum value of all LAI_obs plus twice the standard deviation. We selected the wide distribution of the parameters so that the SVR

model can be trained on a diverse set of data points to reduce bias. Fixed values of sun and view geometry on each observation date were used, taken from the satellite image metadata. Moreover, a modelled dry soil spectrum from 400 to 2500 nm, default in prosail 2.5.2 package (Jacquemoud, Baret, and Hanocq 1992), was considered in the PROSAIL model inversion. It should be noted that the use of a soil spectrum is mainly relevant in sparse vegetation and, therefore, has less impact in dense canopies.

(2) The sample space used in this study consisted of 50,000 input parameter vectors generated randomly from defined input parameters' distributions. For each input parameter set (vector), the PROSAIL model was used to simulate the corresponding TOC reflectance (ranging from 400 to 2500 nm with 1 nm spectral resolution). The simulated reflectance vectors were then resampled to the four VNIR bands of the satellite data, chosen for LAI simulation, using a satellite spectral response function (SRF). The satellite TOC reflectance also includes the uncertainty that arises from several factors, such as instrument noise, radiometric calibration, atmospheric and geometric corrections, and the radiative transfer model itself (Hauser et al. 2021; Sun et al. 2022; Verger, Baret, and Camacho 2011). For LAI simulation, these uncertainties were taken into account by applying random Gaussian noise to the simulated and resampled TOC reflectance.

(3) We trained 50 SVR models following Hauser et al. (2021). Each SVR model was trained using 1000 randomly selected LAI values from the input parameter vectors, along with their corresponding simulated and resampled TOC reflectance vectors.

Table 2. The lower bound (LB) and upper bound (UB) of the PROSAIL input parameters, along with their sources/references used in this study. σ_{allobs} is the standard deviation of all LAI observations (LAI$_{obs}$).

Parameters	Symbol	Unit	LB	UB	Sources/References
Leaf chlorophyll a +b content	C_{ab}	µg cm^{-2}	0	100	Bayat, van der Tol, and Verhoef (2020); Verhoef, van der Tol, and Middleton (2018)
Carotenoids	C_{ca}	µg cm^{-2}	0	30	30% of C_{ab}
Equivalent water thickness	C_w	cm	0.001	0.045	Sun et al. (2022); Bayat, van der Tol, and Verhoef (2020); Verhoef, van der Tol, and Middleton (2018)
Leaf dry matter content	C_{dm}	g cm^{-2}	0.001	0.04	Sun et al. (2022); Hauser et al. (2021)
Anthocyanins	C_{anth}	µg cm^{-2}	0	10	Hauser et al. (2021); Féret et al. (2017)
Leaf browm pigment	C_{bp}	unitless	0	0.3	Bayat, van der Tol, and Verhoef (2020); Verhoef, van der Tol, and Middleton (2018)
Leaf area index	LAI	m ^{2}/m ^{2}	0	12	UB = max(all LAI$_{obs}$) + 2 × σ_{allobs}
Leaf structural parameter	N	unitless	1	3.5	Verhoef, van der Tol, and Middleton (2018)
Average leaf inclination angle	ALIA		10	80	Verhoef (1998); Verhoef, van der Tol, and Middleton (2018)
Soil Brightness parameter	psoil	unitless	0	0.9	Verhoef, van der Tol, and Middleton (2018)
Hot spot parameter	q	m/m	0.001	0.5	Verhoef, van der Tol, and Middleton (2018)
Observer zenith angle	OZA	deg			
Sun zenith angle	SZA	deg			Fixed value derived from Satellite orbit characteristics and swath
Relative azimuth angle	psi	deg			

To ensure unbiased sampling from finite populations, we used sampling with replacement to randomly select the LAI values.

(4) The final step in simulating LAI from satellite data involved inverting satellite TOC reflectance to LAI (hereafter, LAI_{sim}). To accomplish this, the trained 50 SVR models were applied to each pixel of satellite data. The output of this process generated 50 LAI_{sim} values for each pixel. To produce a representative LAI_{sim} value of a pixel, the mean of the 50 generated values was calculated. In this way, using both PlantScope and Sentinel-2 satellite data, LAI_{sim} map was created over the entire study area for each crop phenological phase (Table 1).

We chose to use only the VNIR bands at 10 m resolution of Sentinel-2 data to train our SVR models in step 3. There were two reasons for this choice: (1) these bands were sufficient to obtain LAI_{sim} as NIR is the most sensitive band to vegetation greenness and LAI, and (2) these bands match the ones used by all PlanetScope sensors (Table 1), which allows for a fair comparison of LAI_{sim} derived from both satellite data.

3.4. Statistical evaluation of simulated LAI

We extracted LAI_{sim} from both satellite data at each of the sampling locations (Figure 1b) on each crop phenological phase in 2020 and 2021 (Table 1). We employed Kling-Gupta efficiency (KGE) and Root mean square error (RMSE) statistical criteria to evaluate the accuracy of LAI_{sim} against LAI_{obs}. KGE considers a balanced optimization of product bias, variability, and correlation to quantify the error efficiently (Gupta et al. 2009). KGE and RMSE are calculated as follows:

$$KGE = \sqrt{(r-1)^2 + \left(\frac{\sigma_{sim}}{\sigma_{obs}} - 1\right)^2 + \left(\frac{\mu_{sim}}{\mu_{obs}} - 1\right)^2}, \qquad (1)$$

$$RMSE = \sqrt{\frac{1}{n}\sum_{i=1}^{n}\left((LAI_{obs})_i - (LAI_{sim})_i\right)^2}, \qquad (2)$$

where r is the linear correlation between LAI_{obs} and LAI_{sim}, σ_{obs} and μ_{obs} represent the standard deviation and mean of LAI_{obs} respectively, σ_{sim} and μ_{sim} represent the standard deviation and mean of LAI_{sim}. The ratio of σ and μ describes the variability error and the bias term. The term n represents the number of sampling locations, i.e. 14 in 2020 and 18 in 2021. The KGE criterion can range from $-\infty$ to 1. A KGE value close to 1 indicates a perfect match of simulations to the observations. Positive KGE values are considered 'good', whereas negative KGE values are labelled as 'bad' matches. We considered $-0.41 < KGE \leq 1$ as reasonable accuracy, and $KGE \geq 0.3$ as behavioural simulations with adequate accuracy in LAI_{sim} (Bayat et al. 2024; Knoben, Freer, and Woods 2019). The RMSE criterion has the unit of LAI. A low value of RMSE indicates high accuracy with an optimal value of 0. We considered both KGE and RMSE since KGE offered a relative performance measure, and the latter an absolute one. We also quantified the correlation r criterion, a component of KGE, and R^2 (coefficient of

determination) to demonstrate the degree of linear association between the LAI_{obs} and LAI_{sim}.

3.5. Spatial heterogeneity in simulated LAI

The premise behind simulating LAI from PlanetScope data is that, in comparison to Sentinel-2 data, it may better capture spatial heterogeneity in LAI. To demonstrate this, we employed Rao's Q heterogeneity index (Rao 1982) computation on each LAI_{sim} map (Section 3.3) utilizing the 'rasterdiv' R package (Rocchini et al. 2021). Rao's Q index evaluates the variability of pixels relative to the variability across neighbouring pixels. A moving window approach is used on the image (LAI_{sim} map in this study) until the whole spatial extent is covered. Rao's Q index is calculated from the pixel values inside a moving window and attached to the central pixel. The procedure generates the heterogeneity map over the image's spatial extent. Rao's Q is calculated as:

$$\text{Rao's Q index} = \sum_{i=1}^{N}\sum_{j=1}^{N} d_{ij} \times p_i \times p_j, \tag{3}$$

where p_i and p_j are the relative abundances of ith and j^{th} pixel, and d_{ij} is the distance, such as the Euclidean distance, between the ith and j^{th} pixel in a moving window of pixels N. The relative abundance of a pixel is determined by dividing the actual value of the pixel (which is the value of LAI_{sim}) by the sum of pixel values in a moving window. We chose a moving window of size 3×3 pixels ($N = 9$) in this study. Rao's Q index can take any positive value, with the higher value showing more heterogeneity compared with the neighbouring pixels.

We generated and compared the heterogeneity maps of LAI_{sim} obtained from PlanetScope and Sentinel-2 for each crop phenological phase during the years 2020 and 2021. Our aim was to identify any significant differences in the spatial LAI_{sim} patterns of the crops between the two satellite data and to determine the most effective data for monitoring heterogeneity in crop LAI at the field scale.

4. Results

4.1. Simulated LAI: PlanetScope and Sentinel-2

The scatterplots presented in Figure 2 compare LAI_{sim} values, extracted at the sampling locations, against LAI_{obs} values across both crop phenological phases and years. In 2020, both PlanetScope and Sentinel-2 sensors exhibited strong behavioural performance during the end of stem elongation and flowering phases, with the KGE values significantly surpassing the 0.3 threshold, reaching as high as 0.77 for PlanetScope during the end of stem elongation phase. However, the performance of PlanetScope in 2021 during the end of stem elongation phase showed a decline with a KGE value of 0.38, which was still higher than the threshold. Nonetheless, high KGE values (0.70 and 0.85) during the end of flowering phase for both satellite data indicated a return to strong behavioural performance. Overall, the KGE values reflected the adequate accuracy of LAI_{sim} from both satellite data.
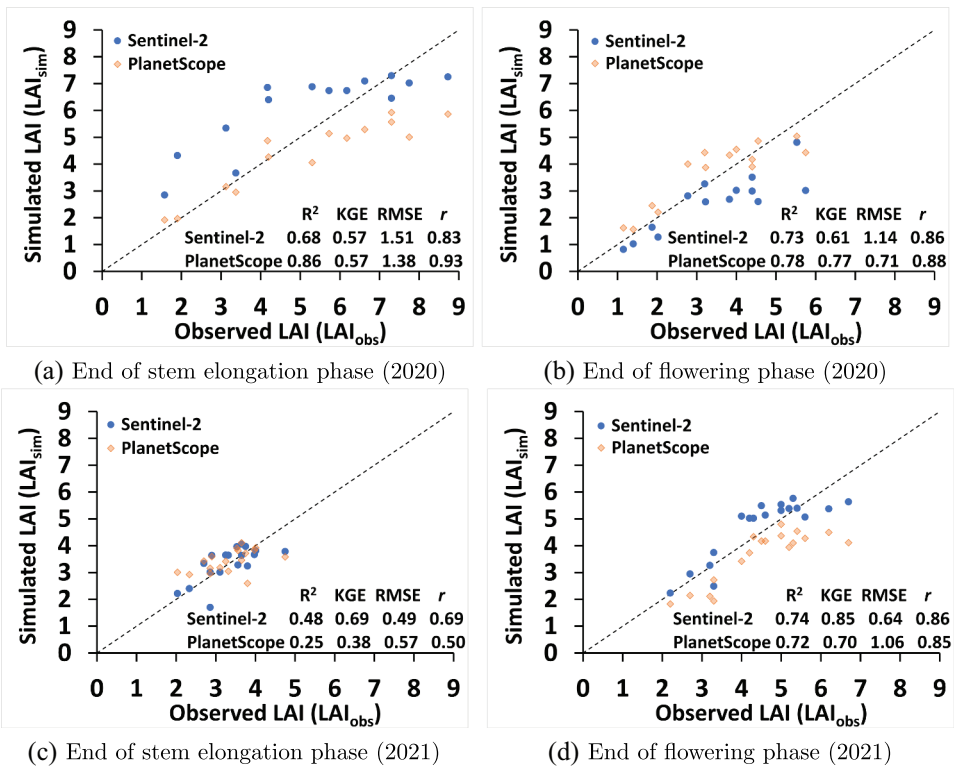
Figure 2. Scatterplots showing the relationship between LAI_{sim} and LAI_{obs} at the sampling locations distributed over the Grossmutz agriculture field across different crop phenological phases of winter triticale crop in 2020 and 2021. Each plot includes a dashed line representing a 1:1 relationship.

For other statistical criteria, PlanetScope showed higher values ($R^2 = 0.86$, $r = 0.93$) compared to Sentinel-2 ($R^2 = 0.68$, $r = 0.83$) during the end of stem elongation phase 2020. This suggested that PlanetScope aligned more closely and linearly with LAI_{obs}. The RMSE values also supported this, being lower for PlanetScope (1.38) than for Sentinel-2 (1.51). Nonetheless, Sentinel-2 performance can still be considered satisfactory in this crop phenological phase. During the end of flowering phase in 2020, both satellite data showed improved performance compared to the previous phase. However, PlanetScope still maintained a slight edge with higher R^2 and r values of 0.78 and 0.88 compared to Sentinel-2 R^2 and r values of 0.73 and 0.86, respectively. The RMSE value for PlanetScope was also significantly lower at 0.71 compared to Sentinel-2 at 1.41.

Both satellite data exhibited a drop in R^2 and r values during the end of stem elongation phase in 2021. PlanetScope exhibited $R^2 = 0.25$ and $r = 0.50$, while Sentinel-2 performed better with $R^2 = 0.48$ and $r = 0.69$. However, PlanetScope RMSE was higher at 0.57 compared to Sentinel-2 at 0.49, indicating that the LAI_{sim} values were slightly better with PlanetScope. The end of flowering phase in 2021 showed a recovery in the accuracy of LAI_{sim}, and both satellite data showed similar and high values of R^2 (> 0.7) and r (≈ 0.85). However, Sentinel-2 showed a lower RMSE value compared to PlanetScope, indicating higher accuracy in LAI_{sim}.

(a) End of stem elongation phase (2020) (b) End of flowering phase (2020) (c) End of stem elongation phase (2021) (d) End of flowering phase (2021)
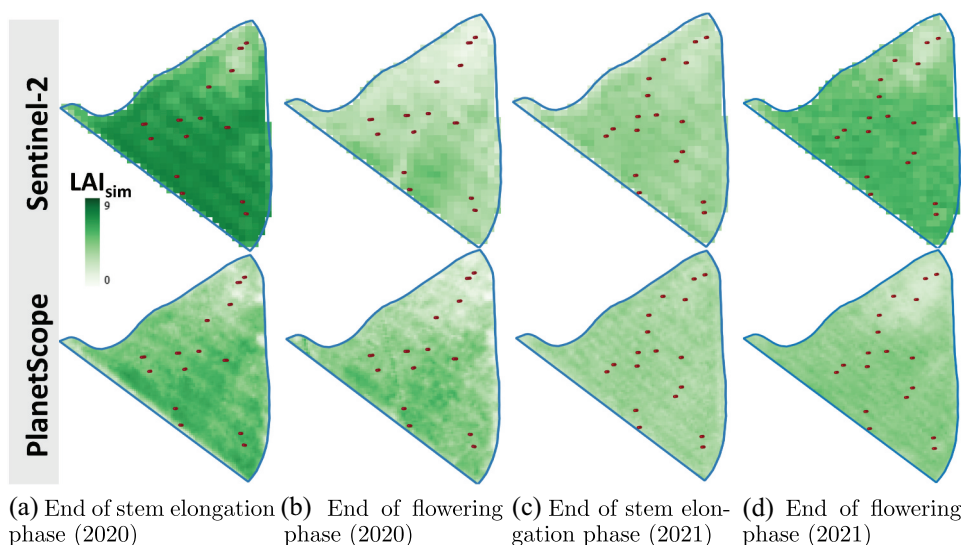
Figure 3. LAI$_{sim}$ maps across different crop phenological phases in 2020 and 2021. Red dots show the sampling locations, 14 in 2020 and 18 in 2021, distributed over the Grossmutz agriculture field.

The maps presented in Figure 3 provide a comprehensive visual representation of the spatial distribution and variation of LAI$_{sim}$ values during different crop phenological phases over a span of two years. The maps indicated a relatively uniform distribution of mid to high LAI$_{sim}$ values across the crop field, with specific areas exhibiting lower LAI$_{sim}$ values. This variance in LAI$_{sim}$ values can be attributed to the soil heterogeneity within the crop field, which causes variable yield conditions (Figure 1b and Section 4.2). Both satellite data showed higher LAI$_{sim}$ values during the end of stem elongation phase in the year 2020, suggesting better crop conditions or growth during that year. However, during the end of flowering phase in 2021, the LAI$_{sim}$ values became comparable to those of the previous year, indicating the recovery of crop growth between the two crop phenological phases.

4.2. Simulated LAI: soil classes

Figure 4 reports the mean and standard deviation (σ) of LAI (LAI$_{sim}$ and LAI$_{obs}$) to examine the influence of three different soil classes (Figure 1b) on LAI development and to assess how well satellite data performed in these three soil classes. The mean and σ were computed based on the LAI values obtained at the sampling locations in each soil class.

Across the crop phenological phases, soil class SC1 generally exhibited the highest mean LAI for both satellite data as well as observations, which aligns with its classification of having high yield potential. The σ error bars are relatively narrow, indicating less variability in LAI and more consistent growing conditions. Soil class SC2 showed a moderate mean LAI, aligning with its medium yield potential. The error bars are marginally wider than in SC1, indicating more variability in crop growth within this class. The soil class SC3 exhibited the lowest mean LAI, which correlates with its low
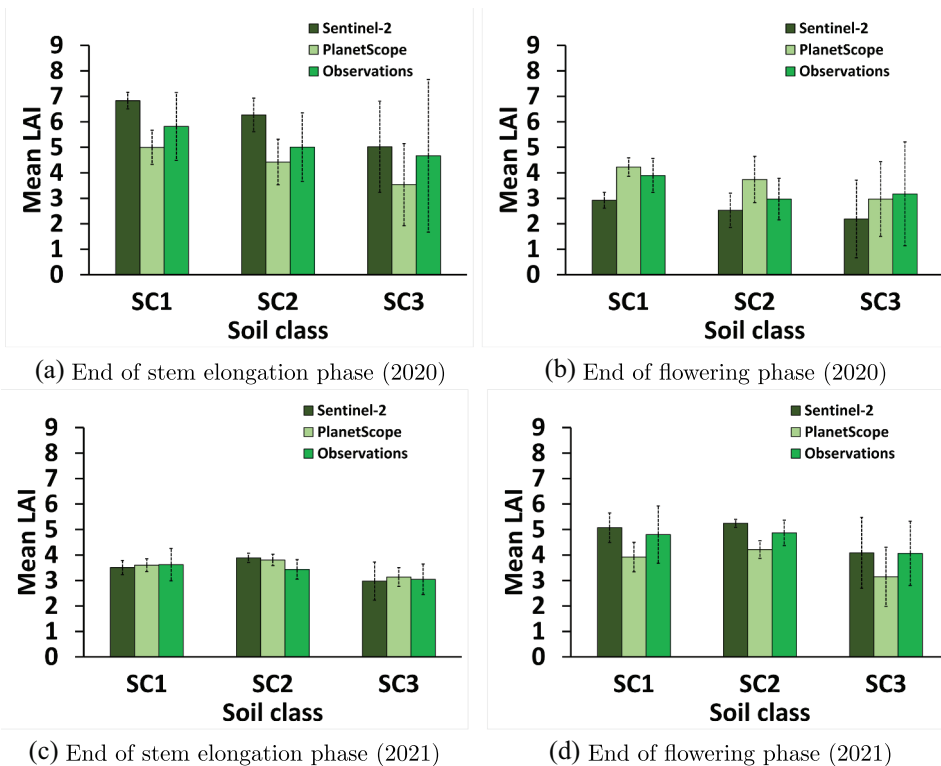
(a) End of stem elongation phase (2020)

(b) End of flowering phase (2020)

(c) End of stem elongation phase (2021)

(d) End of flowering phase (2021)

Figure 4. Bar plots showing the mean LAI (LAI_{sim} and LAI_{obs}) at the sampling points in each of the soil classes (SC1, SC2 and SC3; Figure 1b) during different crop phenological phases. The error bars (dotted lines) represent $\pm 1\sigma$ (standard deviation).

yield potential. The error bars are the widest among the three classes, suggesting the highest variability in growth conditions.

Sentinel-2 generally showed higher mean LAI values compared to those of PlanetScope and observations, particularly in higher yield potential soil (SC1). For instance, during the end of stem elongation phase in 2020, Sentinel-2 reported a mean LAI of 6.83 in SC1, which is higher than both PlanetScope (5.0) and observations (5.82). This trend is evident across both phenological phases. PlanetScope showed lower mean LAI values than Sentinel-2 but is generally closer to the observations. However, the difference between LAI_{obs} and LAI_{sim} were comparable for both satellite data, and these differences ranged from 0.02 to 1.2 across all soil classes and crop phenological phases. Therefore, both satellite data can be considered to perform similarly in terms of mean LAI values in all soil classes.

Both satellite data exhibited lower variability (standard deviation) across all soil classes compared to the observations. However, PlanetScope is closer to the observations in terms of variability across the different soil classes and crop phenological phases. For instance, PlanetScope variability ranged from 0.3 to 0.7 in SC1, which was closer to the range (0.6 to 1.3) exhibited by observations as compared to Sentinel-2 (0.2 to 0.6). In SC2, these ranges were 0.3 to 0.9 for PlanetScope, 0.1 to 0.6 for Sentinel-2, and 0.3 to 1.3 for observations. This suggested that PlanetScope data might be slightly more reliable in terms of capturing the variability in LAI.
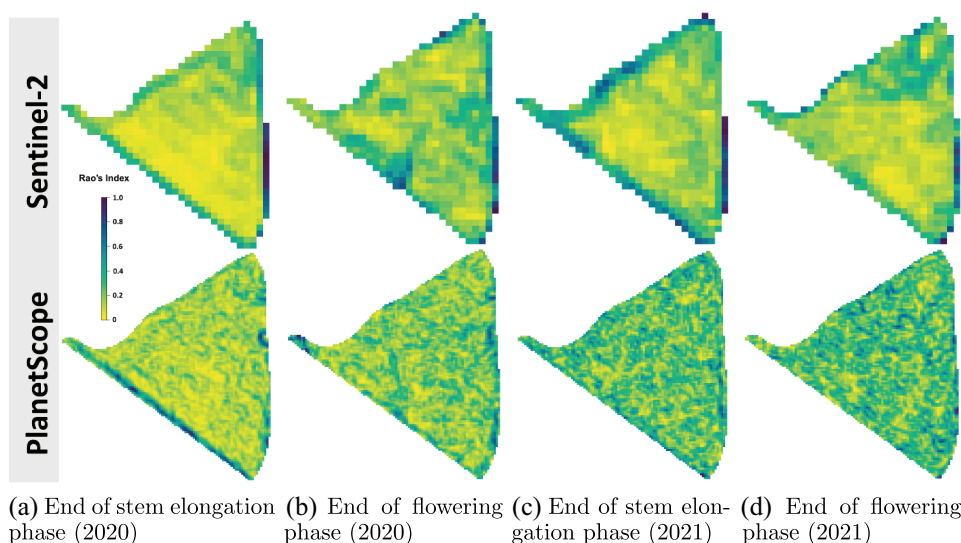
(a) End of stem elongation phase (2020) (b) End of flowering phase (2020) (c) End of stem elongation phase (2021) (d) End of flowering phase (2021)

Figure 5. Rao's Q heterogeneity maps (normalised between 0 and 1) during different crop phenological phases in 2020 and 2021.

4.3. Simulated LAI: heterogeneity analysis

We used the moving window approach and Equation 3 to create a spatial heterogeneity map of LAI_{sim}. Each pixel on the map was assigned a Rao's Q index value. Since Rao's Q index can take any positive value, we normalized the heterogeneity map between 0 and 1, based on the minimum and maximum index values in a map, to allow for a direct comparison between the heterogeneity of LAI_{sim} obtained from PlanetScope and Sentinel-2 data (Figure 5).

Sentinel-2 heterogeneity maps generally showed relatively smoother transitions in Rao's Q index values, with a dominance of yellow and green shades. This indicated moderate heterogeneity levels and a more generalized view of LAI_{sim}. The spatial resolution of 10 meters in Sentinel-2 allowed for a broader overview but less detail in small-scale variations. In contrast, the PlanetScope heterogeneity maps showed more detailed and localized variations in LAI_{sim} heterogeneity. These maps are characterized by a more textured appearance, with a mix of blue, green, and yellow patches indicating varying levels of heterogeneity across the field. The finer resolution of 3 m in PlanetScope captured smaller patches of variability within the crop field, which are not as discernible in the Sentinel-2 heterogeneity maps.

Across the years and phenological phases, the patterns of heterogeneity changed, reflecting the dynamic nature of crop growth and development. The end of stem elongation phase maps generally showed less heterogeneity compared to the end of flowering phase maps, which could be due to the uniform growth during stem elongation and more varied characteristics of leaf area at the flowering stage.

5. Discussion

Our study demonstrated that a hybrid inversion approach can reliably simulate LAI from high- and mid-resolution satellite data, such as PlanetScope and Sentinel-2, across

different crop phenological phases and years. This approach synergistically combines the detailed physical modelling capabilities of PROSAIL, which simulates the interaction of light among the canopy, with the robust machine learning techniques of SVR, known for its effectiveness in handling non-linear relationships between input and output and high-dimensional spaces created by several input parameters. Our study is consistent with previous studies where the hybrid inversion approach, though combined with different machine learning approaches, outperformed in terms of accuracy for crop LAI simulated from Sentinel-2 data (Rosso et al. 2022; Upreti et al. 2019; Verrelst et al. 2015). The fusion of PlanetScope and Sentinel-2 for LAI simulation using hybrid inversion was also highlighted in some studies (Johansen et al. 2022; Sadeh et al. 2021). Nevertheless, we provided a direct comparison between Sentinel-2 and PlanetScope data for LAI simulation. We selected a wide uniform distribution of each PROSAIL input parameter (Table 2) as non-informative priors. The selection was based on the range proposed in the literature, without considering the crop types. We did this to ensure that our input parameters were only marginally dependent on the field observations. Although we implemented the hybrid inversion approach to a single crop type using non-informative priors, the reliable LAI simulation indicated that it could potentially be applied to another crop type with minimal inputs from field observations.

We validated simulated LAI (LAI_{sim}) with multiple point-scale observed LAI (LAI_{obs}) distributed across the study area. Using multiple point-scale observations as a reference for validating the related pixel in satellite-derived LAI products, even those with coarser resolutions such as MODIS, is a widely accepted practice. This approach is also supported by community-agreed best practices and established validation protocols (Bayat et al. 2021; Fernandes et al. 2014). Therefore, employing point-scale LAI_{obs} remains a valid and reliable method for evaluating remote sensing-based simulations, including those derived from both PlanetScope and Sentinel-2. These satellites have a significantly higher spatial resolution than MODIS and align closely with the ground reference sampling points. However, the difference in scale between the 1 m^2 field sampling plot (Section 3.1) and the 10 m Sentinel-2 pixels may introduce some uncertainty in the validation. To reduce this effect, we averaged multiple ground samples within each plot across the study area to reduce the influence of local heterogeneity. Nonetheless, a degree of scale mismatch remains unavoidable and should be investigated in future studies.

The LAI_{sim} from 2020 and 2021 revealed fluctuations in the performance of PlanetScope and Sentinel-2. The differences in accuracy observed between both satellite data across time periods are likely due to sensor-specific characteristics and spatial resolution differences. Although the same four VNIR spectral bands (Section 3.2) were used for LAI simulation, variations in radiometric calibration and atmospheric correction procedures can affect the retrieved TOC reflectance values. Sentinel–2 benefits from rigorous sensor calibration and exhibits low uncertainty in radiometry and geometry (Gascon et al. 2017; Lamquin et al. 2019), whereas PlanetScope images, despite their high spatial and temporal resolution, are subject to radiometric inconsistencies inherent in their satellite sensors (Dias et al. 2024; Leach, Coops, and Obrknezev 2019). Previous studies have also highlighted differences in band behaviour and calibration between PlanetScope and Sentinel-2, emphasizing the need for cross-sensor harmonization to reduce discrepancies (Baldin and Marco Casella 2025; Sadeh

et al. 2021). In addition, spatial resolution differences may also contribute: PlanetScope finer 3 m resolution increases sensitivity to within–field heterogeneity, whereas Sentinel–2 10 m resolution integrates over a broader area. These combined factors provide plausible explanations for the observed discrepancies between Sentinel–2 and PlanetScope data in this study.

We observed that PlanetScope generally provided more accurate and correlated LAI_{sim} in 2020, its performance slightly dropped in 2021, particularly during the end of stem elongation phase. In 2020, PlanetScope LAI_{sim} were more tightly distributed around the 1:1 line (Figure 2), especially at the end of flowering phase, indicating minimal bias and stronger agreement with LAI_{obs} with higher KGE, lower RMSE, and stronger R^2 and r. Sentinel-2, although slightly less accurate in 2020, showed more consistent performance across the two years and slightly better statistical criteria in some instances in 2021. Sentinel-2 exhibited more dispersion in 2020, but LAI_{sim} aligned more closely with the 1:1 line across both phenological phases in 2021, reflecting improved and more consistent KGE, RMSE, R^2 and r. However, the temporal dynamics of LAI_{sim}, either from PlanetScope or Sentinel-2, was generally consistent with the development of leaf area of winter triticale across different phenological phases. At the end of stem elongation phase, LAI_{sim} is typically moderate to high because this phase is associated with vigorous vegetative growth; the canopy tends to become denser, resulting in increased leaf area. At the end of flowering phase, the LAI_{sim} generally starts to decline. Flowering marks the transition from vegetative to reproductive growth, and energy resources are diverted towards grain development rather than foliage expansion. As the crop shifts its focus towards seed filling, leaf senescence may occur, leading to a reduction in leaf area and, consequently, a decrease in LAI_{sim}.

The variation in LAI_{obs} across different soil classes can be partially explained by soil moisture (SM) at 15 cm and 45 cm depths, measured during critical crop development stages at the Grossmutz agriculture field (Habib-Ur-Rahman et al. 2022). They found that SM for soil class SC1 was higher than for SC3. The average SM in the top layers (0–45 cm) over all sampling points showed a significantly strong association with LAI_{obs} as well as the total dry mass, and plant height of the triticale crop, especially during the end of stem elongation and the end of the flowering phase. Differences in soil texture across the soil classes resulted in variations in water retention potential and water availability to the crop, ultimately affecting plant growth and LAI. In this study, the same soil-class effect is evident in LAI_{sim} from both PlanetScope and Sentinel-2 images, showing higher values on the soil class SC1 with greater available water capacity (AWC) and progressively lower values on the sandy texture soil class SC3 with low AWC. The comparison of mean LAI (LAI_{sim}) at the sampling locations within the different soil classes revealed a similar performance of both satellite data in terms of magnitude (Section 4.2). Whereas the standard deviation (σ) showed that the variability in LAI_{sim} is generally lower for Sentinel-2, suggesting more uniformity of leaf area over the crop field. PlanetScope, while showing lower mean LAI_{sim}, exhibited higher variability indicating its sensitivity to variations in soil and vegetation conditions.

The comparison between Sentinel-2 and PlanetScope Rao's Q heterogeneity index maps further revealed significant differences in the level of detail and variability captured by each satellite's resolution. PlanetScope's higher resolution provided a more nuanced

understanding of crop condition variability, which could be crucial for precision agriculture practices such as variable rate applications at the field scale. Such applications incorporating PlanetScope variability can help reduce uniform application rates of agriculture inputs such as water, fertilizer, and soil amendments to maximize photosynthesis and carbon fixation in crops. This can enhance overall crop yield and sustainability and can improve the efficiency of crop carbon sequestration (Janzen et al. 2022; Jin et al. 2017; Johansen et al. 2022; Tiefenbacher et al. 2021). PlanetScope LAI$_{sim}$ can effectively support the management of agricultural carbon sequestration strategies, contributing significantly to the mitigation of climate change impacts. Sentinel-2, while simulating less spatial variability in LAI$_{sim}$ compared to PlanetScope, captured the magnitude and trend in crop leaf area across different crop phenological phases. Sentinel-2 offers broad coverage and frequent revisit time, which makes it excellent for regional to national carbon sequestration studies, which focus on broad trends and changes over large areas. A recent study (Wijmer et al. 2024) also highlighted the large-scale simulation of agriculture carbon storage utilizing Sentinel-2 data.

Harmonizing multi-temporal LAI from different satellite platforms and generating fused time-series products is an essential and valuable direction, especially for applications like precision agriculture that require continuous and consistent monitoring. In this study, however, our primary objective was to evaluate the differences in LAI$_{sim}$ and mapping performance between the two satellite data sources, serving as a foundational step towards understanding the intra-field variability detection and their heterogeneity analysis. This assessment is critical before attempting harmonization, as it highlights sensor-specific biases, spatial-temporal resolution differences, and retrieval inconsistencies that could affect data fusion outcomes.

6. Conclusions

We examined a hybrid inversion approach to simulate leaf area index (LAI) from high- and mid-resolution satellite data, such as PlanetScope and Sentinel-2, in a small agriculture field. Both data showed similar performance in capturing the LAI magnitude. However, Sentinel-2 showed lower within-field variability in LAI compared with PlanetScope, as demonstrated by the spatial heterogeneity maps. The PlanetScope variability aligned more consistently with the soil classes, which belong to different yield potentials across the field. We included two crop phenological phases of two years due to the corresponding availability of the observed LAI. However, we ensured that the input parameters for LAI simulations were independent of the crop types and phases. Because LAI is a direct and spatially explicit indicator of canopy biomass and photosynthetic capacity, this study, through the comparison of LAI simulated from PlanetScope and Sentinel-2 data, represents a first step towards more data-driven agricultural system applications. The high-resolution LAI maps generated in this study successfully captured within-field heterogeneity, demonstrating their value for improving yield estimation, guiding site-specific management decisions, and providing a practical basis for plot-level carbon accounting. Nevertheless, future studies could also focus on longitudinal assessments of LAI simulation performance using PlanetScope and Sentinel-2 data over multiple years and across various crop phenological phases. This could provide a deeper understanding of the temporal variations in satellite data performance, allowing for the identification of

underlying factors impacting accuracy and consistency. Likewise, comparative analyses of LAI simulation performance under different environmental conditions and crop types could further elucidate the strengths and limitations of each satellite data source for monitoring crop LAI dynamics. Eventually, an essential next step would be the implementation of a method that harmonizes PlanetScope and Sentinel-2 data across spatial, spectral, and temporal domains. Once this consistency is achieved, the two data can then be fused, combining PlanetScope's fine spatial detail with Sentinel-2's spectral richness to produce denser and more consistent LAI time series, thereby enhancing their practical utility in precision-agriculture decision-making.

Acknowledgement

Disclosure statement

No potential conflict of interest was reported by the author(s)

Funding

ORCID

Rahul Raj http://orcid.org/0000-0002-7871-6629
Bagher Bayat http://orcid.org/0000-0002-7761-9544
Ahsan Raza http://orcid.org/0000-0002-7856-7176
Thomas Gaiser http://orcid.org/0000-0002-5820-2364
Harry Vereecken http://orcid.org/0000-0002-8051-8517
Carsten Montzka http://orcid.org/0000-0003-0812-8570

Data availability

The data that support the findings of this study are available from the corresponding author, R. Raj, upon reasonable request.

References

Baldin, C. M., and V. Marco Casella. 2025. "Comparison of PlanetScope and Sentinel-2 Spectral Channels and Their Alignment via Linear Regression for Enhanced Index Derivation." *Geosciences* 15 (5). https://doi.org/10.3390/geosciences15050184.

Bauer, J., and N. Aschenbruck. 2018. "Design and Implementation of an Agricultural Monitoring System for Smart Farming." *2018 IoT Vertical and Topical Summit on Agriculture - Tuscany (IOT Tuscany)*: 1–6. https://doi.org/10.1109/IOT-TUSCANY.2018.8373022.

Bayat, B., F. Camacho, J. Nickeson, M. Cosh, J. Bolten, H. Vereecken, and C. Montzka. 2021. "Toward Operational Validation Systems for Global Satellite-Based Terrestrial Essential Climate Variables."

International Journal of Applied Earth Observation and Geoinformation 95:102240. https://doi.org/10.1016/j.jag.2020.102240.

Bayat, B., R. Raj, A. Graf, H. Vereecken, and C. Montzka. 2024. "Comprehensive Accuracy Assessment of Long-Term Geostationary SEVIRI-MSG Evapotranspiration Estimates Across Europe." *Remote Sensing of Environment* 301:113875. https://doi.org/10.1016/j.rse.2023.113875.

Bayat, B., C. Van der Tol, and W. Verhoef. 2016. "Remote Sensing of Grass Response to Drought Stress Using Spectroscopic Techniques and Canopy Reflectance Model Inversion." *Remote Sensing* 8 (7). https://doi.org/10.3390/rs8070557.

Bayat, B., C. van der Tol, and W. Verhoef. 2018. "Integrating Satellite Optical and Thermal Infrared Observations for Improving Daily Ecosystem Functioning Estimations During a Drought Episode." *Remote Sensing of Environment* 209:375–394. https://doi.org/10.1016/j.rse.2018.02.027.

Bayat, B., C. van der Tol, and W. Verhoef. 2020. "Retrieval of Land Surface Properties from an Annual Time Series of Landsat TOA Radiances During a Drought Episode Using Coupled Radiative Transfer Models." *Remote Sensing of Environment* 238:110917. https://doi.org/10.1016/j.rse.2018.09.030.

Bleiholder, H., E. Weber, P. D. Lancashire, C. Feller, L. Buhr, M. Hess, H. Wicke, H. Hack, U. Meier, and R. Klose. 2001. "Growth Stages of Mono-and Dicotyledonous Plants, BBCH Monograph." *Federal Biological Research Centre for Agriculture and Forestry, Berlin/Braunschweig, Germany, BBCH Monograph* 158.

Burroughs, C. H., C. M. Montes, C. A. Moller, N. G. Mitchell, A. M. Michael, B. Peng, H. Kimm, et al. 2022. "Reductions in Leaf Area Index, Pod Production, Seed Size, and Harvest Index Drive Yield Loss to High Temperatures in Soybean." *Journal of Experimental Botany* 74 (5): 1629–1641. https://doi.org/10.1093/jxb/erac503.

DeLay, N. D., N. M. Thompson, and J. R. Mintert. 2022. "Precision Agriculture Technology Adoption and Technical Efficiency." *Journal of Agricultural Economics* 73 (1): 195–219. https://doi.org/10.1111/1477-9552.12440.

Dias, R. L. S., R. Santos Silva Amorim, D. D. da Silva, E. Inácio Fernandes-Filho, G. Vieira Veloso, and R. Henrique Fonseca Macedo. 2024. "Relative Radiometric Normalization for the PlanetScope Nanosatellite Constellation Based on Sentinel-2 Images." *Remote Sensing* 16 (21): 4047. 21. https://doi.org/10.3390/rs16214047.

Fang, H., F. Baret, S. Plummer, and G. Schaepman-Strub. 2019. "An Overview of Global Leaf Area Index (LAI): Methods, Products, Validation, and Applications." *Reviews of Geophysics* 57 (3): 739–799. https://doi.org/10.1029/2018RG000608.

Feret, J.-B., and F. de Boissieu. 2024. *Prosail: PROSAIL Leaf and Canopy Radiative Transfer Model and Inversion Routines*. R Package Version 2.5.2. https://gitlab.com/jbferet/prosail.

Féret, J.-B., and F. de Boissieu. 2024. "Prospect: An R Package to Link Leaf Optical Properties with Their Chemical and Structural Properties with the Leaf Model PROSPECT." *Journal of Open Source Software* 9 (94): 6027. https://doi.org/10.21105/joss.06027.

Féret, J.-B., A. A. Gitelson, S. D. Noble, and S. Jacquemoud. 2017. "PROSPECT-D: Towards Modeling Leaf Optical Properties Through a Complete Lifecycle." *Remote Sensing of Environment* 193:204–215. https://doi.org/10.1016/j.rse.2017.03.004.

Fernandes, R., S. Plummer, J. Nightingale, F. Baret, F. Camacho, H. Fang, S. Garrigues, et al. 2014. "Global Leaf Area Index Product Validation Good Practices. Version 2.0." In *Best Practice for Satellite-Derived Land Product Validation*, edited by G. Schaepman-Strub, M. Roman, and J. Nickeson, 76. Land Product Validation Subgroup (WGCV/CEOS). https://doi.org/10.5067/doc/ceoswgcv/lpv/lai.002.

Gara, T. W., R. Darvishzadeh, A. K. Skidmore, T. Wang, and M. Heurich. 2019. "Evaluating the Performance of PROSPECT in the Retrieval of Leaf Traits Across Canopy Throughout the Growing Season." *International Journal of Applied Earth Observation and Geoinformation* 83:101919. https://doi.org/10.1016/j.jag.2019.101919.

Gascon, F., C. Bouzinac, O. Thèpaut, M. Jung, B. Francesconi, J. Louis, V. Lonjou, et al. 2017. "Copernicus Sentinel-2A Calibration and Products Validation Status." *Remote Sensing* 9 (6): 584. https://doi.org/10.3390/rs9060584.

Gupta, H. V., H. Kling, K. K. Yilmaz, and G. F. Martinez. 2009. "Decomposition of the Mean Squared Error and NSE Performance Criteria: Implications for Improving Hydrological Modelling." *Journal of Hydrology* 377 (1): 80–91. https://doi.org/10.1016/j.jhydrol.2009.08.003.

Habib-Ur-Rahman, M., A. Raza, H. E. Ahrends, H. Hüging, and T. Gaiser. 2022. "Impact of In-Field Soil Heterogeneity on Biomass and Yield of Winter Triticale in an Intensively Cropped Hummocky Landscape Under Temperate Climate Conditions." *Precision Agriculture* 23 (3): 912–938. https://doi.org/10.1007/s11119-021-09868-x.

Hauser, L. T., J.-B. Féret, N. An Binh, N. van der Windt, Â. F. Sil, J. Timmermans, N. A. Soudzilovskaia, and P. M. van Bodegom. 2021. "Towards Scalable Estimation of Plant Functional Diversity from Sentinel-2: In-Situ Validation in a Heterogeneous (Semi-)Natural Landscape." *Remote Sensing of Environment* 262:112505. https://doi.org/10.1016/j.rse.2021.112505.

Jacquemoud, S., and F. Baret. 1990. "PROSPECT: A Model of Leaf Optical Properties Spectra." *Remote Sensing of Environment* 34 (2): 75–91. https://doi.org/10.1016/0034-4257(90)90100-Z.

Jacquemoud, S., F. Baret, and J. F. Hanocq. 1992. "Modeling Spectral and Bidirectional Soil Reflectance." *Remote Sensing of Environment* 41 (2): 123–132. https://doi.org/10.1016/0034-4257(92)90072-R.

Jacquemoud, S., W. Verhoef, F. Baret, C. Bacour, P. J. Zarco-Tejada, G. P. Asner, C. François, and S. L. Ustin. 2009. "Prospect+Sail Models: A Review of Use for Vegetation Characterization." *Remote Sensing of Environment* 113:S56–S66. https://doi.org/10.1016/j.rse.2008.01.026.

Janzen, H. H., K. J. van Groenigen, D. S. Powlson, T. Schwinghamer, and J. J. W. van Groenigen. 2022. "Photosynthetic Limits on Carbon Sequestration in Croplands." *Geoderma* 416:115810. https://doi.org/10.1016/j.geoderma.2022.115810.

Jin, Z., R. Prasad, J. Shriver, and Q. Zhuang. 2017. "Crop Model-and Satellite Imagery-Based Recommendation Tool for Variable Rate N Fertilizer Application for the US Corn System." *Precision Agriculture* 18 (5): 779–800. https://doi.org/10.1007/s11119-016-9488-z.

Johansen, K., M. G. Ziliani, R. Houborg, T. E. Franz, and M. F. McCabe. 2022. "Cubesat Constellations Provide Enhanced Crop Phenology and Digital Agricultural Insights Using Daily Leaf Area Index Retrievals." *Scientific Reports* 12 (1): 5244. https://doi.org/10.1038/s41598-022-09376-6.

Kimm, H., K. Guan, C. Jiang, B. Peng, L. F. Gentry, S. C. Wilkin, S. Wang, et al. 2020. "Deriving High-Spatiotemporal-Resolution Leaf Area Index for Agroecosystems in the U.S. Corn Belt Using Planet Labs CubeSat and STAIR Fusion Data." *Remote Sensing of Environment* 239:111615. https://doi.org/10.1016/j.rse.2019.111615.

Knoben, W. J. M., J. E. Freer, and R. A. Woods. 2019. "Technical Note: Inherent Benchmark or Not? Comparing Nash–Sutcliffe and Kling–Gupta Efficiency Scores." *Hydrology and Earth System Sciences* 23 (10): 4323–4331. https://doi.org/10.5194/hess-23-4323-2019.

Lamquin, N., E. Woolliams, V. Bruniquel, F. Gascon, J. Gorroño, Y. Govaerts, V. Leroy, et al. 2019. "An Inter-Comparison Exercise of Sentinel-2 Radiometric Validations Assessed by Independent Expert Groups." *Remote Sensing of Environment* 233:111369. https://doi.org/10.1016/j.rse.2019.111369.

Laskari, M., G. Menexes, I. Kalfas, I. Gatzolis, and C. Dordas. 2022. "Water Stress Effects on the Morphological, Physiological Characteristics of Maize (Zea Mays L.), and on Environmental Cost." *Agronomy* 12 (10). https://doi.org/10.3390/agronomy12102386.

Leach, N., N. C. Coops, and N. Obrknezev. 2019. "Normalization Method for Multi-Sensor High Spatial and Temporal Resolution Satellite Imagery with Radiometric Inconsistencies." *Computers and Electronics in Agriculture* 164:104893. https://doi.org/10.1016/j.compag.2019.104893.

Liao, J., Y. Zang, X. Luo, Z. Zhou, Y. Zang, P. Wang, and A. John Hewitt. 2020. "The Relations of Leaf Area Index with the Spray Quality and Efficacy of Cotton Defoliant Spraying Using Unmanned Aerial Systems (UASs)." *Computers and Electronics in Agriculture* 169:105228. https://doi.org/10.1016/j.compag.2020.105228.

Liu, T., S.-B. Duan, N. Liu, B. Wei, J. Yang, J. Chen, and L. Zhang. 2024. "Estimation of Crop Leaf Area Index Based on Sentinel-2 Images and PROSAIL-Transformer Coupling Model." *Computers and Electronics in Agriculture* 227:109663. https://doi.org/10.1016/j.compag.2024.109663.

Lowenberg-DeBoer, J., and B. Erickson. 2019. "Setting the Record Straight on Precision Agriculture Adoption." *Agronomy Journal* 111 (4): 1552–1569. https://doi.org/10.2134/agronj2018.12.0779.

Lower, L., J. Cunniffe, J. J. Cheng, and W. Joe Sagues. 2022. "Coupling Circularity with Carbon Negativity in Food and Agriculture Systems." *Journal of Agricultural Safety and Health* 65 (4): 849–864. https://doi.org/10.13031/ja.14908.

Nevalainen, O., O. Niemitalo, I. Fer, A. Juntunen, T. Mattila, O. Koskela, J. Kukkamäki, et al. 2022. "Towards Agricultural Soil Carbon Monitoring, Reporting, and Verification Through the Field Observatory Network (FION)." *Geoscientific Instrumentation, Methods and Data Systems* 11 (1): 93–109. https://doi.org/10.5194/gi-11-93-2022.

Pasqualotto, N., S. Falanga Bolognesi, O. Rosario Belfiore, J. Delegido, G. D'Urso, and J. Moreno. 2019. "Canopy Chlorophyll Content and LAI Estimation from Sentinel-2: Vegetation Indices and Sentinel-2 Level-2A Automatic Products Comparison." 2019 IEEE International Workshop on Metrology for Agriculture and Forestry (MetroAgriFor), Portici, Italy. 301–306. https://doi.org/10.1109/MetroAgriFor.2019.8909218.

Paul, M., A. Rajib, M. Negahban-Azar, A. Shirmohammadi, and P. Srivastava. 2021. "Improved Agricultural Water Management in Data-Scarce Semi-Arid Watersheds: Value of Integrating Remotely Sensed Leaf Area Index in Hydrological Modeling." *Science of the Total Environment* 791:148177. https://doi.org/10.1016/j.scitotenv.2021.148177.

Planet Team. 2023. *Planet Imagery Product Specifications*, Berlin, Germany: Panet Labs Inc. Accessed on February 28, 2023. https://assets.planet.com/docs/Planet_Combined_Imagery_Product_Specs_letter_screen.pdf.

Raj, R., B. Bayat, P. Lukeš, L. Šigut, and L. Homolová. 2020. "Analyzing Daily Estimation of Forest Gross Primary Production Based on Harmonized Landsat-8 and Sentinel-2 Product Using SCOPE Process-Based Model." *Remote Sensing* 12 (22). https://doi.org/10.3390/rs12223773.

Rao, C. R. 1982. "Diversity and Dissimilarity Coefficients: A Unified Approach." *Theoretical Population Biology* 21 (1): 24–43. https://doi.org/10.1016/0040-5809(82)90004-1.

Raza, A., H. Ahrends, M. Habib-Ur Rahman, H. Hüging, and T. Gaiser. 2022. "Using the Taguchi Experimental Design for Assessing Within-Field Variability of Surface Run-Off and Soil Erosion Risk." *Science of the Total Environment* 828:154567. https://doi.org/10.1016/j.scitotenv.2022.154567.

Rocchini, D., E. Thouverai, M. Marcantonio, M. Iannacito, D. Da Re, M. Torresani, G. Bacaro, et al. 2021. "Rasterdiv-An Information Theory Tailored R Package for Measuring Ecosystem Heterogeneity from Space: To the Origin and Back." *Methods in Ecology and Evolution* 12 (6): 1093–1102. https://doi.org/10.1111/2041-210X.13583.

Román, C., M. Peris, J. Esteve, M. Tejerina, J. Cambray, P. Vilardell, and S. Planas. 2022. "Pesticide Dose Adjustment in Fruit and Grapevine Orchards by DOSA3D: Fundamentals of the System and On-Farm Validation." *Science of the Total Environment* 808:152158. https://doi.org/10.1016/j.scitotenv.2021.152158.

Rosso, P., C. Nendel, N. Gilardi, C. Udroiu, and F. Chlebowski. 2022. "Processing of Remote Sensing Information to Retrieve Leaf Area Index in Barley: A Comparison of Methods." *Precision Agriculture* 23 (4): 1449–1472. https://doi.org/10.1007/s11119-022-09893-4.

Sachin, K. S., A. Dass, S. Dhar, G. A. Rajanna, T. Singh, S. Sudhishri, M. S. Sannagoudar, A. K. Choudhary, H. L. Kushwaha, B. R. Praveen, S. Prasad, V. K. Sharma, V. Pooniya, P. Krishnan, M. Khanna, R. Singh, T. Varatharajan, K. Kumari, K. Nithinkumar, Aye-Aye San, and A. D. Devi. 2023. "Sensor-Based Precision Nutrient and Irrigation Management Enhances the Physiological Performance, Water Productivity, and Yield of Soybean Under System of Crop Intensification." *Frontiers in Plant Science* 14. https://doi.org/10.3389/fpls.2023.1282217.

Sadeh, Y., X. Zhu, D. Dunkerley, J. P. Walker, Y. Zhang, V. S. M. Offer Rozenstein, and K. Chenu. 2021. "Fusion of Sentinel-2 and PlanetScope Time-Series Data into Daily 3m Surface Reflectance and Wheat LAI Monitoring." *International Journal of Applied Earth Observation and Geoinformation* 96:102260. https://doi.org/10.1016/j.jag.2020.102260.

Shi, J., X. Wu, M. Zhang, X. Wang, Q. Zuo, X. Wu, H. Zhang, and A. Ben-Gal. 2021. "Numerically Scheduling Plant Water Deficit Index-Based Smart Irrigation to Optimize Crop Yield and Water

Use Efficiency." *Agricultural Water Management* 248:106774. https://doi.org/10.1016/j.agwat.2021.106774.

Steinwart, I., and P. Thomann. 2017. "LiquidSVM: A Fast and Versatile SVM Package." *arXiv preprint arXiv:1702.06899*. https://doi.org/10.48550/arXiv.1702.06899.

Sun, J., L. Wang, S. Shi, Z. Li, J. Yang, W. Gong, S. Wang, and T. Tagesson. 2022. "Leaf Pigment Retrieval Using the PROSAIL Model: Influence of Uncertainty in Prior Canopy-Structure Information." *Crop Journal* 10 (5): 1251–1263. Crop phenotyping studies with application to crop monitoring. https://doi.org/10.1016/j.cj.2022.04.003.

Tiefenbacher, A., T. Sandén, H.-P. Haslmayr, J. Miloczki, W. Wenzel, and H. Spiegel. 2021. "Optimizing Carbon Sequestration in Croplands: A Synthesis." *Agronomy* 11 (5). https://doi.org/10.3390/agronomy11050882.

Upreti, D., W. Huang, W. Kong, S. Pascucci, S. Pignatti, X. Zhou, H. Ye, and R. Casa. 2019. "A Comparison of Hybrid Machine Learning Algorithms for the Retrieval of Wheat Biophysical Variables from Sentinel-2." *Remote Sensing* 11 (5). https://doi.org/10.3390/rs11050481.

Verger, A., F. Baret, and F. Camacho. 2011. "Optimal Modalities for Radiative Transfer-Neural Network Estimation of Canopy Biophysical Characteristics: Evaluation Over an Agricultural Area with CHRIS/PROBA Observations." *Remote Sensing of Environment* 115 (2): 415–426. https://doi.org/10.1016/j.rse.2010.09.012.

Verhoef, W. 1998. "Theory of Radiative Transfer Models Applied in Optical Remote Sensing of Vegetation Canopies." PhD thesis, Wageningen, The Netherlands. Wageningen University & Research. https://edepot.wur.nl/210943.

Verhoef, W., and H. Bach. 2007. "Coupled Soil–Leaf-Canopy and Atmosphere Radiative Transfer Modeling to Simulate Hyperspectral Multi-Angular Surface Reflectance and TOA Radiance Data." *Remote Sensing of Environment* 109 (2): 166–182. https://doi.org/10.1016/j.rse.2006.12.013.

Verhoef, W., L. Jia, Q. Xiao, and Z. Su. 2007. "Unified Optical-Thermal Four-Stream Radiative Transfer Theory for Homogeneous Vegetation Canopies." *IEEE Transactions on Geoscience & Remote Sensing* 45 (6): 1808–1822. https://doi.org/10.1109/TGRS.2007.895844.

Verhoef, W., C. van der Tol, and E. M. Middleton. 2018. "Hyperspectral Radiative Transfer Modeling to Explore the Combined Retrieval of Biophysical Parameters and Canopy Fluorescence from FLEX – Sentinel-3 Tandem Mission Multi-Sensor Data." *Remote Sensing of Environment* 204:942–963. https://doi.org/10.1016/j.rse.2017.08.006.

Verrelst, J., J. Pablo Rivera, F. Veroustraete, J. Muñoz-Marí, J. G. P. W. Clevers, G. Camps-Valls, and J. Moreno. 2015. "Experimental Sentinel-2 LAI Estimation Using Parametric, Non-Parametric and Physical Retrieval Methods – A Comparison." *ISPRS Journal of Photogrammetry & Remote Sensing* 108:260–272. https://doi.org/10.1016/j.isprsjprs.2015.04.013.

Wang, Y., Y. Yuan, F. Yuan, S. Tahir Ata-Ui-Karim, X. Liu, Y. Tian, Y. Zhu, W. Cao, and Q. Cao. 2023. "Evaluation of Variable Application Rate of Fertilizers Based on Site-Specific Management Zones for Winter Wheat in Small-Scale Farming." *Agronomy* 13 (11). https://doi.org/10.3390/agronomy13112812.

Wijmer, T., A. Al Bitar, L. Arnaud, R. Fieuzal, and E. Ceschia. 2024. "Agricarbon-EO V1.0.1: Large-Scale and High-Resolution Simulation of Carbon Fluxes by Assimilation of Sentinel-2 and Landsat-8 Reflectances Using a Bayesian Approach." *Geoscientific Model Development* 17 (3): 997–1021. https://doi.org/10.5194/gmd-17-997-2024.

Yang, R., L. Liu, Q. Liu, X. Li, L. Yin, X. Hao, Y. Ma, and Q. Song. 2022. "Validation of Leaf Area Index Measurement System Based on Wireless Sensor Network." *Scientific Reports* 12 (1): 4668. https://doi.org/10.1038/s41598-022-08373-z.

Zérah, Y., S. Valero, and J. Inglada. 2024. "Physics-Constrained Deep Learning for Biophysical Parameter Retrieval from Sentinel-2 Images: Inversion of the PROSAIL Model." *Remote Sensing of Environment* 312:114309. https://doi.org/10.1016/j.rse.2024.114309.